doi:10.1016/j.jmb.2006.03.063 J. Mol. Biol. (2006) 359, 741–753

JMB

Available online at www.sciencedirect.com

SCIENCE DIRECT®

ELSEVIER

Structure–Stability–Activity Relationship in Covalently Cross-linked *N*-Carbamoyl D-Amino acid Amidohydrolase and *N*-Acylamino acid Racemase

Wei-Chun Chiu[1], Ji-Yu You[1], Jai-Shin Liu[1], Shih-Kuang Hsu[2] Wen-Hwei Hsu[2], Chien-Hua Shih[3], Jenn-Kang Hwang[3] and Wen-Ching Wang[1]*

[1]*Institute of Molecular and Cellular Biology & Department of Life Science, National Tsing Hua University, HsinChu Taiwan, 30013, ROC*

[2]*Institute of Molecular Biology National Chung Hsing University, Taichung Taiwan, 30013, ROC*

[3]*Institute of Bioinformatics & Department of Biological Science and Technology National Chiao Tung University, HsinChu, Taiwan 30013, ROC*

**Corresponding author*

N-Acylamino acid racemase (NAAAR) and *N*-carbamoyl-D-amino-acid amidohydrolase (D-NCAase) are important biocatalysts for producing enantiopure α-amino acids. NAAAR forms an octameric assembly and displays induced fit movements upon substrate binding, while D-NCAase is a tetramer that does not change conformation in the presence of a ligand. To investigate the effects of introducing potentially stabilizing S–S bridges in these different multimeric enzymes, cysteine residues predicted to form inter or intra-subunit disulfide bonds were introduced by site-directed mutagenesis. Inter-subunit S–S bonds were formed in two NAAAR variants (A68C-D72C and P60C-Y100C) and two D-NCAase variants (A302C and P295C-F304C). Intra-subunit S–S bonds were formed in two additional NAAAR variants (E149C-A182C and V265C). Crystal structures of NAAARs variants show limited deviations from the wild-type overall tertiary structure. An *apo* A68C-D72C subunit differs from the wild-type enzyme, in which it has an ordered lid loop, resembling ligand-bound NAAAR. The structures of A222C and A302C D-NCAases are nearly identical to the wild-type enzyme. All mutants with inter-subunit bridges had increases in thermostability. Compared with the wild-type enzyme, A68C-D72C NAAAR showed similar k_{cat}/K_m ratios, whereas mutant D-NCAases demonstrated increased k_{cat}/K_m ratios at high temperatures (A302C: 4.2-fold at 65 °C). Furthermore, molecular dynamic simulations reveal that A302C substantially sustains the fine-tuned catalytic site as temperature increases, achieving enhanced activity.

Keywords: NAAAR, *N*-acylamino acid racemase; D-NCAase, *N*-carbamoyl D-amino acid amidohydrolase; disulfide bond; thermostability; activity

Introduction

The structure–activity relationship of enzymes is interesting from both fundamental and application perspectives. Pioneering works on small enzymes such as T4 lysozyme suggest that introduction of point mutations can greatly enhance protein stability.[1] During the past years, directed evolution using methods including random mutagenesis, site-directed mutagenesis and DNA shuffling has been widely employed to screen or select optimized enzymes with desired properties.[2–4] There are, however, successful mutants that contain mutation sites that are difficult to rationalize, especially in the absence of three-dimensional structures.[5,6]

Comparative investigations of proteins from extreme thermophilic and mesophilic organisms, on the other hand, reveal structural features crucial for a protein operating at high temperatures.[7–9] These include superior protein rigidity, optimization of the hydrophobic packing in the interior, enhanced networks from salt bridges and hydrogen bonds, and a decrease in surface hydrophobicity.

Abbreviations used: NAAAR, *N*-acylamino acid racemase; D-NCAase, *N*-carbamoyl D-amino acid amidohydrolase; NAQ, *N*-acetyl-glutamine; r.m.s.d., root-mean-square deviation.

E-mail address of the corresponding author: wcwang@life.nthu.edu.tw

Mutants of high thermostability have thus been obtained with reasonable success rates based on the following principles: (i) to increase entropic stabilization by introducing disulfide bridges, salt bridges, and/or ionic interactions; (ii) to shorten or strengthen solvent-exposed loops and termini; (iii) to enhance the extent of secondary structure formation; and (iv) to lower the entropy of unfolded states of the protein structure.[6,7,10,11] Quaternary interactions in oligomeric enzymes also contribute to thermostability.[12–16] Introduction of additional inter-subunit S–S bridges or interactions has been shown to increase the thermostability of some multimeric enzymes.[17–22]

Despite these efforts, there are still many questions about the structure–stability–activity interrelationship for oligomeric enzymes during catalysis. To approach this issue, we sought to investigate *N*-acylamino acid racemase (NAAAR) from *Deinococcus radiodurans*, which undergoes an induced-fit movement upon substrate binding.[23] NAAAR catalyzes the racemization of *N*-acylamino acids and has been used to produce optically active methionine in an immobilized NAAAR-aminoacylase reaction process, which has potential industrial applications.[24] The crystal structure of NAAAR reveals a homo-octamer with 4-fold symmetry. Each subunit consists of a capping domain and a $(\beta/\alpha)_7\beta$ barrel domain, characteristic of the enolase architecture.[23,25] Analysis of the *apo* and NAAAR·*N*-acetyl-L-glutamine (NAQ)·Mg^{2+} complex structures reveals essential residues involved in catalysis: K170 and K269 are two catalysts to abstract an α-proton of a carboxylate, while D195, E220, and D245 are Mg^{2+}-binding residues.[23] Moreover, in the liganded structure, the capping domain and barrel domain move toward each other, resulting in a narrowed pocket, and a disordered-to-ordered transition occurs in which a lid loop closes over the substrate in the complex structure.[23]

We also investigated an industrial enzyme, *N*-carbamoyl-D-amino acid amidohydrolase (D-NCAase) that catalyzes the conversion of *N*-carbamoyl-D-amino acids into D-amino acids including D-phenylglycine and D-*p*-hydroxyphenylglycine, the basic building blocks of β-lactam antibiotics.[26,27] The crystal structure of D-NCAase from *Agrobacterium radiobacter* reveals a homo-tetramer of 222 symmetry and each subunit demonstrates a four-layer α-β-β-α architecture, structurally belonging to the nitrilase superfamily.[28,29] A C172-E47-K127 catalytic triad within a solvent-accessible pocket is evident in liganded structures.[30] As opposed to the considerable conformational changes seen in NAAAR, there are limited changes in the active-site arrangement as well as in the overall conformation between *apo* and liganded D-NCAase.

In the present study, NAAAR and D-NCAase mutants with additional S–S disulfide bridges were generated by site-directed mutagenesis. Structures, stabilities and activity properties of variants were characterized. Our results demonstrate that an NAAAR mutant structure (A68C-D72C) has an "ordered" lid loop and liganded-like conformation, even without a ligand. All mutants with additional S–S bridges had increased thermostability. Strikingly, D-NCAase mutants, particularly A302C, had increased stabilities and activities at higher temperatures. Molecular dynamic simulations provide the molecular bases of the fine-tuned catalytic pockets for A302C at 300 K, 338 K and 350 K.

Results and Discussion

Production of NAAAR and D-NCAase mutants

Possible sites for disulfide bridges were predicted primarily using the MODIP program based on geometric considerations.[31] Within a tightly associated dimer A1-C1 of NAAAR,[23] two pairs of residues were predicted as candidates for forming inter-subunit disulfide bridges after mutation to cysteine: the A68 and D72 pair and P60 and Y100 pair. Mutation of these residues to cysteine would likely yield cross-linking bridges between the capping domains (Table 1). Of potential sites for intra-subunit disulfide bridges (37 in the capping domain and 56 in the barrel domain of *apo* NAAAR), nine were chosen for site-directed mutagenesis: five were in the capping domain (V48C-R120C, G50C-A113C, M56C-E65C, A119C-G353C, and G127C-T313C) and four in the barrel domain (E149C-A182C, G163C-D343C, V265C, and Y218C). V265C and Y218C were predicted to pair with the naturally occurring C243, respectively. The 11 NAAAR mutants were produced by site-directed mutagenesis. Expression of these mutants showed that G50C-A113C and A119C-G353C were produced in inclusion bodies while the other nine were expressed as soluble proteins. The nine soluble variants were purified by affinity chromatography and were >95% pure as judged by SDS-PAGE analysis (data not shown). Moreover, each of the purified mutant proteins displayed a nearly identical CD spectrum to that of the wild-type enzyme (data not shown), indicating no major secondary structural changes upon the substitution.

Using the same approach, four D-NCAase mutants were generated that were expected to form inter-subunit disulfide links: P295C-F304C was predicted to form two inter-subunit disulfide bridges, while P178C, A222C, and A302C would each form a disulfide bridge with the symmetry-related molecule in the dimer (Table 1). Based on the structure, all these residues are located in the close proximity to the 2-fold axis in the tightly associated dimer. P295, A302 and F304 are situated at the C-terminal segment, while P178 and A222 are in helix 5 and helix 6 of the exterior α layer, respectively. The four mutants were generated and purified by affinity chromatography. Each of the purified D-NCAases was >95% pure as judged by SDS-PAGE analysis (data not shown). CD analysis of each mutant revealed a nearly identical profile to that of the wild-type enzyme (data not shown).

Table 1. Characterization of NAAAR and D-NCAase mutants

Mutant	Predicted S–S bonds	Position	Expression	Relative activity (%)[a]	Formed S–S bonds[b]
A. *NAAAR*					
A68C-D72C	Inter	Capping (H_{C1}/H_{C1})	Normal	100.0	Yes
P60C-Y100C	Inter	Capping (S_{C4}-H_{C1} Loop/H_{C2}-H_{C3} loop)	Normal	0	Yes
E149C-A182C	Intra	Barrel (H_{B1}/H_{B2})	Normal	88.4	Yes
V265C	Intra	Barrel (S_{B6}/S_{B5})	Normal	39.1	Yes
Y218C	Intra	Barrel (S_{B4}/S_{B5})	Normal	34.8	No
G127C-T313C	Intra	Capping (H_{C4}/H_{B7}-S_{B8} loop)	Normal	93.6	No
V48C-R120C	Intra	Capping (S_{C4}/H_{C3})	Normal	0	ND[c]
M56C-E65C	Intra	Capping (S_{C4}-H_{C1} loop/H_{C1})	Normal	0	ND
G163C-D343C	Intra	Barrel (H_{B1}-S_{B2} Loop/S_{B8}-S_{C7} loop)	Normal	0	ND
G50C-A113C	Intra	Capping (S_{C4}/H_{C3})	Insoluble	ND	ND
A119C-G353C	Intra	Capping (H_{C3}/S_{C7}-H_{C5} loop)	Insoluble	ND	ND
B. *D-NCAase*					
P295C-F304C	Inter	C-end/C-end	Normal	107.3	Yes
A302C	Inter	C-end/C-end	Normal	123.9	Yes
P178C	Inter	H5/H5	Normal	ND	No
A222C	Inter	H6/H6	Normal	ND	No

[a] For NAAAR variants, the relative activity of the wild-type enzyme using *N*-acetyl-L-methionine as the substrate was taken as 100%. For D-NCAase variants, the relative activity of the wild-type enzyme using *N*-carbamoyl-D-*p*-hydroxyphenylglycine as the substrate was taken as 100%.
[b] The formation of the expected S–S bridges was determined by SDS-PAGE with or without the reducing agent, crystal structural analysis and/or MALDI-TOF mass spectra analysis.
[c] ND, not determined.

Formation of S–S bonds in NAAAR and D-NCAase mutants

SDS-PAGE analysis and mass spectrum analysis were used to analyze disulfide bond formation in the inter-subunit and intra-subunit mutants, respectively. Under reducing conditions containing β-mercaptoethanol, two inter-subunit NAAAR mutants (A68C-D72C and P60C-Y100C) migrated to positions corresponding to a molecular mass of ~40 kDa, similar to that of the wild-type enzyme (Figure 1(a)). In the absence of the reducing agent, freshly purified inter-subunit mutants shifted to a higher apparent molecular mass (~80 kDa), suggesting that A68C-D72C and P60C-Y100C formed covalent inter-subunit S–S bridges.

Among the NAAAR mutants designed to form intra-subunit disulfide bonds, only V265C and E149C-A182C form the predicted bonds. The presence of the intra-subunit S–S bond in V265C was demonstrated by MALDI-TOF mass spectra analysis after trypsin digestion. An obvious signal at m/z of 2831 Da was present in the standard V265C sample but not in that with dithiothreitol treatment (50 mM). This m/z value is the expected value from two linked fragments (residues 240–255 and residues 257–269) and indicates the formation of the expected intra-subunit S–S bond (Table 1). The disulfide bond in E149C-A182C was observed in the crystal structure (discussed below). In contrast, there is no expected disulfide bond in either the Y218C or G127C-T313C mutants as shown by the crystal structures (discussed below). Disulfide bond formation was not determined for insoluble or inactive mutants.

Similarly, for D-NCAase, P295C-F304C and A302C mutants shifted to a position of higher molecular apparent molecular mass (~70 kDa) under non-reducing conditions in SDS-PAGE, while the other mutants (P178C and A222C) did not, suggesting that only P295C-F304C and A302C

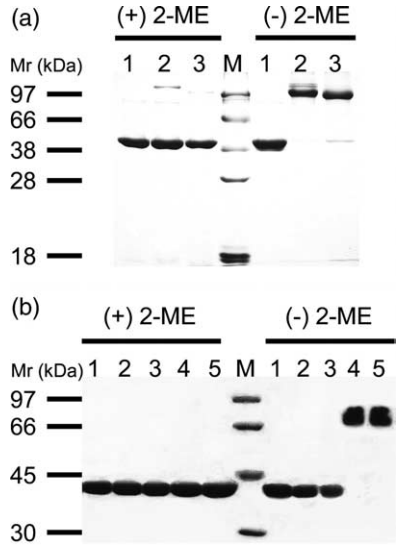

Figure 1. SDS-PAGE analysis of purified NAAAR (a) and D-NCAase (b) mutants under non-reducing or reducing conditions. Each of purified mutant proteins (~5 μg) treated with (+) or without (−) 2-mercaptoethanol was subjected to SDS-10% (w/v) PAGE analysis. (a) Lane 1, NAAAR wild-type; lane 2, P60C-Y100C mutant; lane 3, A68C-D72C mutant. (b) Lane 1, D-NCAase wild-type; lane 2, P178C mutant; lane 3, A222C mutant; lane 4, P295C-F304C mutant; lane 5, A302C mutant.

formed the predicted covalently linked dimers (Table 1).

Crystal structures of NAAARs (A68C-D72C, E149C-A182C, G127C-T313C and Y218C)

We obtained crystals of four NAAAR mutants and determined their structures using molecular replacement methods (Table 2). The substituted side-chain electron density in each mutant was clearly visible. Like the wild-type NAAAR, each of these mutants reveals four molecules (A, B, C and D) related by three non-crystallographic 2-fold axes per asymmetric unit.[23] The refinement statistics of the four structures are given in Table 2.

Each mutant structure, as expected, demonstrates an octameric assembly with 4-fold symmetry, $(AC)_4$ or $(BD)_4$ (Figure 2(a)).[23] Analysis of the monomeric subunit of each mutant also reveals an architecture having a capping domain that consists of eight β strands (S_{C1}–S_{C8}) and five α-helices (H_{C1}–H_{C5}) and a central barrel domain that consists of eight β strands (S_{B1}–S_{B8}) and seven α-helices (H_{B1}–H_{B7}) (Figure 2(b)). The A68C-D72C structure clearly defines two inter-subunit disulfide bridges with S–S distances of 2.06 Å and 2.04 Å between A–C dimers (Figure 2(c)). The E149C-A182C structure also shows an intra-subunit disulfide bond (S–S distance = 2.03 Å, 2.01 Å, 2.03 Å, and 2.04 Å in A, B, C and D chains, respectively). On the other hand, Y218C and G127C-T313C structures reveal that the S atoms of the predicted paired cysteine residues point away from each other, disallowing the formation of a disulfide bridge in each case.

Superposition of each mutant with the wild-type structure reveals that the two mutant structures that lack new disulfide bonds (Y218C and G127C-T313C) show modest deviations in the overall C^α atoms (root-mean-square deviation (r.m.s.d.) of the overall C^α atoms: 0.19 Å and 0.16 Å, respectively). E149C-A182C also displays an overall identical structure (r.m.s.d. of the overall C^α atoms: 0.47 Å). The highest deviation is seen for the C subunits between the *apo* A68C-D72C and the wild-type NAAARs (0.88 Å). Of interest, the untraceable "lid" loop (residues 24–33) in the wild-type *apo* NAAAR structure is now ordered and well defined in the C and D subunits, although it is still absent in A and B subunits in the *apo* A68C-D72C structure. Such a disordered-to-ordered conformational change of the lid loop resembles that seen in a comparison between the *apo* and substrate-bound wild-type structures.[23] Superposition of the A–C dimers of the wild-type and mutant *apo* structures based on the optimized alignment of their A subunits reveals that there is very limited conformational change for the superimposed A subunits, while there are higher deviations in the barrel domains for the superimposed C subunits (data not shown).

Table 2. Crystallographic data

Data collection and phasing	NAAAR					D-NCAase	
Data set	A68C-D72C	A68C-D72C·NAQ	E149C-A182C	G127C-T313C	Y218C	A302C	A222C
Space group	*P*4	*P*4	*P*4	*P*4	*P*4	$P2_1$	$P2_1$
Cell dimensions							
a (Å)	115.64	116.18	116.50	116.13	116.51	70.22	69.38
b (Å)	115.64	116.18	116.50	116.13	116.51	69.46	68.10
c (Å)	120.77	120.82	120.69	120.54	120.23	139.16 $\beta = 95.89°$	138.19 $\beta = 96.08°$
Wavelength (Å)	0.9800	1.5418	1.5418	1.5418	1.5418	1.5418	1.5418
Resolution (Å)	30.0–2.4	30.0–2.2	30.0–2.2	30.0–2.0	30.0–2.5	30.0–2.3	30.0–2.4
Highest resolution shell (Å)	2.49–2.40	2.28–2.20	2.28–2.20	2.07–2.00	2.59–2.50	2.38–2.30	2.49–2.40
Completeness (%)[a]	99.4 (99.8)	99.2 (98.4)	99.1 (98.7)	97.1 (95.3)	99.7 (99.8)	95.6 (95.3)	94.8 (93.6)
Average I/σ (I)	7.3 (2.9)	10.0 (3.5)	9.2 (4.0)	8.7 (2.3)	5.8 (2.9)	10.4 (2.9)	10.7 (3.1)
R_{merge} (%)[b]	10.8 (46.0)	9.2 (45.4)	9.2 (41.3)	9.1 (49.3)	13.4 (45.1)	7.0 (38.4)	9.5 (50.6)
Solvent content (%)	50.9	51.4	51.6	51.2	51.4	47.6	48.1
Refinement							
Resolution range (Å)	30.0–2.4	30.0–2.2	30.0–2.2	30.0–2.0	30.0–2.5	30.0–2.3	30.0–2.4
Protein atoms	11,232	11,262	11,056	11,068	11,040	9568	9568
Solvent atoms	678	705	1293	893	763	285	403
R factor[c]	0.170	0.189	0.166	0.182	0.162	0.178	0.168
R_{free}[d]	0.207	0.228	0.203	0.227	0.208	0.219	0.208
r.m.s.d. bond length (Å)[e]	0.011	0.010	0.011	0.012	0.012	0.010	0.011
r.m.s.d. bond angles (°)	1.363	1.199	1.281	1.299	1.402	1.315	1.381
Estimated coordinate error (Å)	0.301	0.231	0.208	0.180	0.342	0.333	0.335

[a] Values in parentheses refer to statistics in the highest-resolution shell.
[b] $R_{merge} = \sum |I_{obs} - \langle I \rangle| / \sum I_{obs}$.
[c] $R = \sum |F_{obs} - F_{calc}| / \sum F_{obs}$, where F_{obs} and F_{calc} are the observed and calculated structure-factor amplitudes, respectively.
[d] R_{free} was computed using 5% of the data assigned randomly.
[e] r.m.s.d., root mean square deviation.

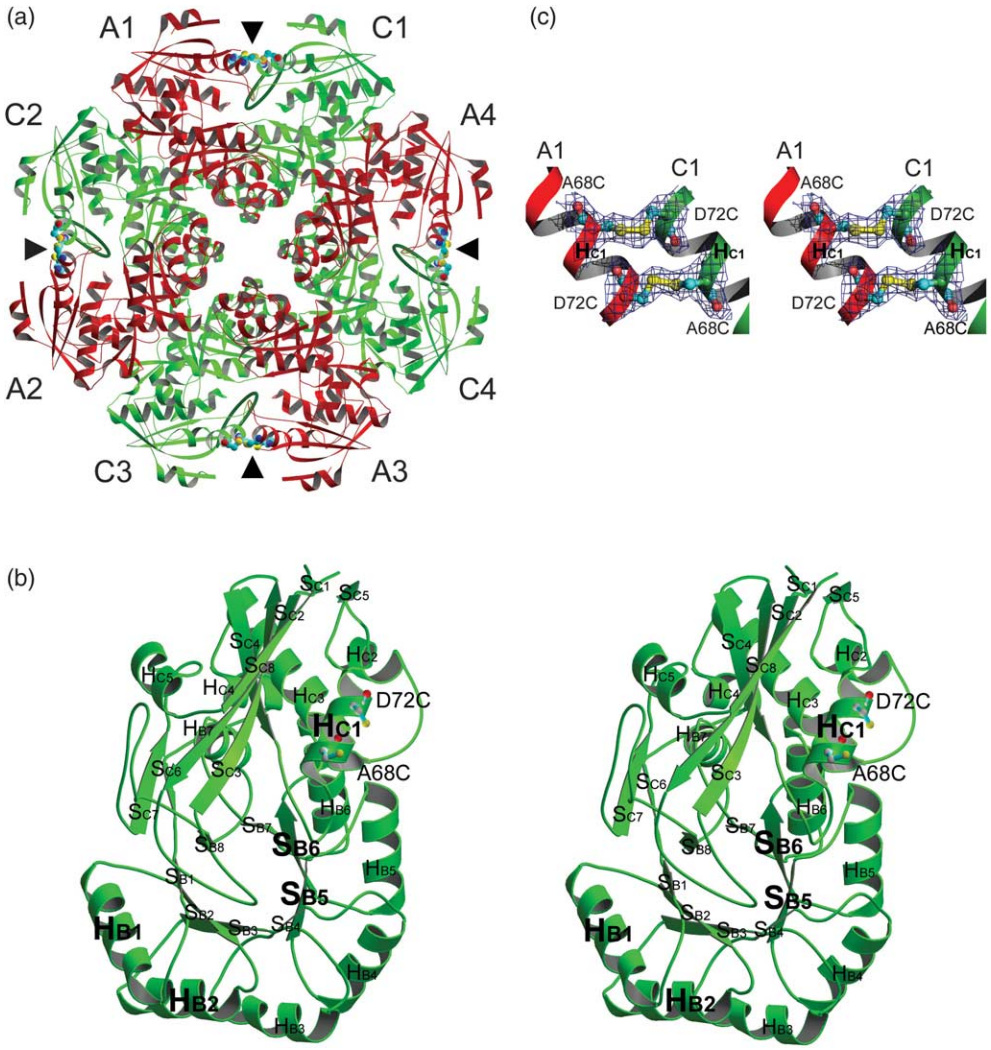

Figure 2. (a) Ribbon representation of the octameric A68C-D72C NAAAR structure viewed down the 4-fold axis. (b) Stereo representation of the monomeric A68C-D72C NAAAR structure. (c) Stereo representation of the disulfide bonds at the interface between each A–C dimer of A68C-D72C are depicted as ball-and-stick models, in which the oxygen, nitrogen and sulfur atoms are in red, blue, and yellow, respectively. The $2F_o - F_c$ map is contoured at the 1.0σ level.

Inside the pocket in the *apo* A68C-D72C C subunit, a higher number of solvent molecules are observed than in the *apo* wild-type enzyme. Based on the wild-type NAAAR·NAQ·Mg^{2+} structure, four substrate-binding sub-sites are identified: a metal-binding site, carboxyl group-binding site, side-chain-binding region and lid region.[23] We find that the front edge of the lid interacts considerably with residues around the carboxyl group-binding site: (i) D27 interacts with G144, I145, and K170 *via* 12 interactions (≤3.8 Å) including a strong H bond with I145 (D27(O)-I145(N), 2.74 Å); (ii) T28 interacts with K170 and N197 *via* seven interactions (≤3.8 Å); and (iii) S29 binds to N197 with ten interactions including a H bond (S29(O^{γ})–N197(O), 3.02 Å). Additionally, F30 interacts with M61 and Y62 (three interactions) from the lid region (S_{C4}–H_{C1} loop).

To clarify the conformation of the lid loop in the A68C-D72C mutant when it binds to NAQ, A68C-D72C·NAQ complex crystals were prepared by co-crystallization methods. The complex structure was determined by molecular replacement methods and refined to an *R* value of 18.9% (R_{free} = 22.8%). Inside the binding cleft of the C and D subunits, a piece of partially broken and weak density is observed at a similar position to that of NAQ in the liganded wild-type structure (Figure 3). This density was thus modeled as the NAQ moiety (the C2, C3, N2, and O4 atoms of NAQ are omitted due to the faint signal).

The ternary complex shows the same octameric assembly and overall fold as the liganded wild-type structure. Superposition of liganded subunits (wild-type *versus* A68C-D72C) reveals nearly identical overall structures (Figure 3(a)). Moreover, the lid loop is ordered, showing limited changes in the equivalent C^{α} atom positions as compared with the *apo* A68C-D72C structure (r.m.s.d.: 0.52 Å). NAQ is enclosed into the pocket of the liganded A68C-D72C form, in which the *N*-acetyl group and the carboxyl moiety of NAQ bind to residues near

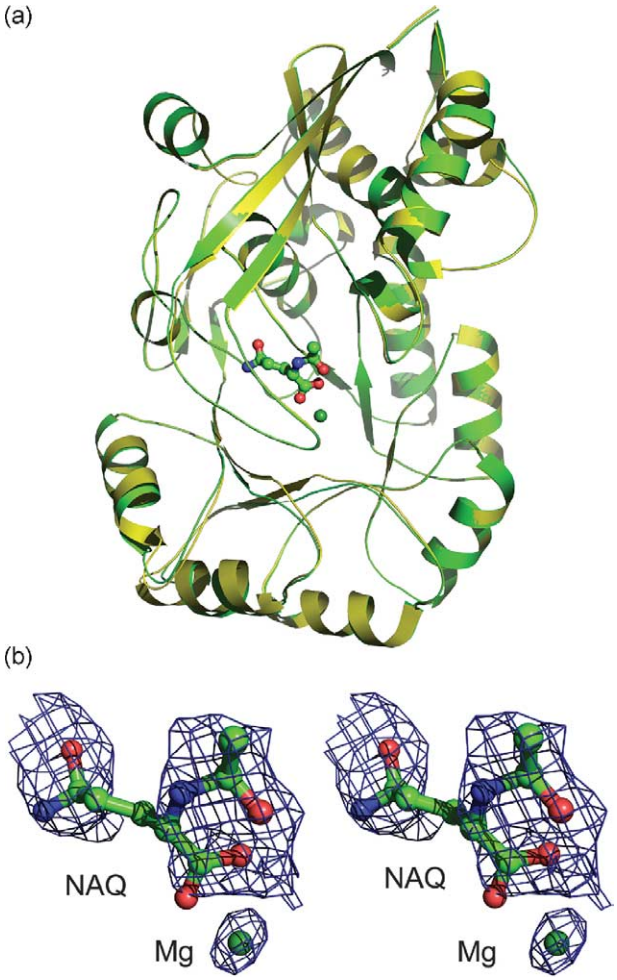

Figure 3. (a) Superimposed C subunits of A68C-D72C·Mg^{2+}·NAQ and NAAAR·Mg^{2+}·NAQ. The C^{α} traces of the wild-type NAAAR and A68C-D72C are shown in yellow and green, respectively. (b) Stereo representation of NAQ shown as ball-and-stick models. The oxygen, nitrogen and Mg atoms are in red, blue, and green, respectively. The $F_o - F_c$ maps of NAQ and Mg^{2+} are contoured at the 1.0σ level.

the lid region and C site, respectively, in a manner similar to that of the wild-type enzyme. No interactions from other crystal lattice contacts with the lid loop are observed in either the *apo* or liganded forms. It is thus most likely that the substituted A68C and D72C residues not only result in the formation of two disulfide bridges between A and C subunits, but also cause restricted flexibility in the linked capping domains. Such a "rigidified" conformation may help the lid loop to contact more extensively with I145 and N197, hence closing up the interface even without the presence of a ligand.

Crystal structures of D-NCAase mutants, A302C and A222C

Of four mutants, crystals of A302C and A222C were obtained and structures were solved with molecular replacement methods and refined to R of 17.8% (R_{free} = 21.9%) and R of 16.8% (R_{free} = 20.8%), respectively (Table 2). The inter-subunit disulfide bridges (S–S distance: 2.04 Å) are seen between the A–B and C–D interfaces of A302C (Figure 4), but not in A222C. Superposition of wild-type and A302C structures shows nearly identical structures (r.m.s.d. of the overall C^{α} atoms: 0.25 Å), indicating that substitution of A302 with Cys does not perturb the conformation.

Covalently cross-linked mutants displayed higher thermostability

To evaluate thermostability, each of the purified mutants was subjected to thermal denaturation and analyzed by CD spectroscopy at 222 nm. An irreversible unfolding profile was seen for each of the wild-type and mutant NAAARs (data not shown). The apparent melting temperatures (T_m)

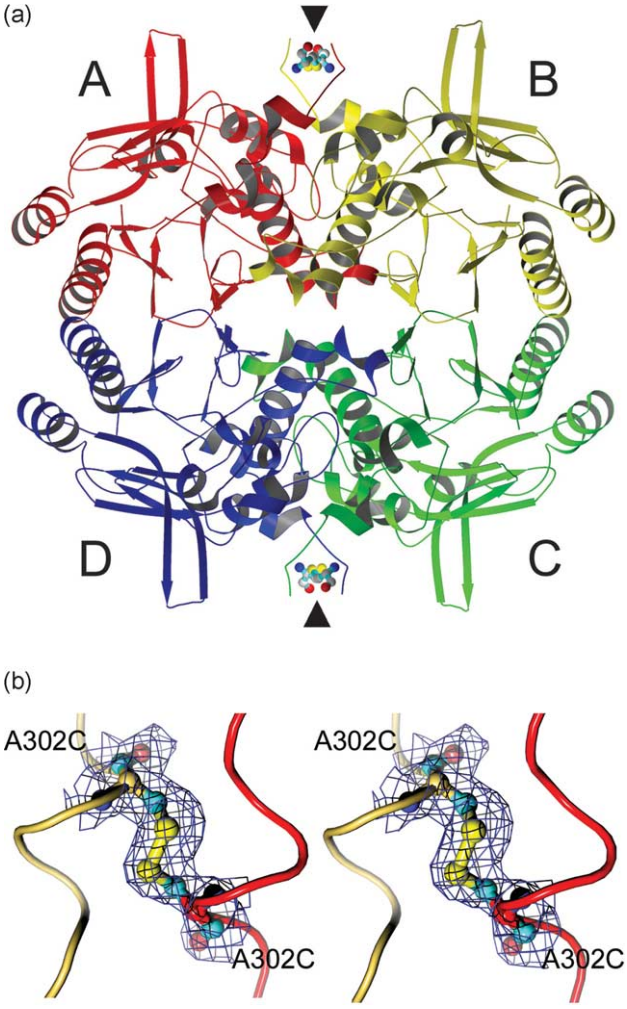

Figure 4. (a) Homotetrameric A302C D-NCAase structure viewed down the A–C (and B–D) dyad axis. Arrows indicates the disulfide bonds. (b) Stereo view of the disulfide bonds in A302C shown as ball-and-stick models. The oxygen, nitrogen and sulfur atoms are in red, blue, and yellow, respectively.

were then obtained from the midpoint of each unfolding curve. As shown in Table 3, variants with the newly introduced S–S bridges (A68C-D72C, P60C-Y100C, E149C-A182C and V265C) exhibited higher T_m values than wild-type NAAAR. It is noted that V265C, which possesses only one intra-subunit S–S bond, had a similar T_m value (78.8 °C) to that of A68C-D72C and P60C-Y100C, which have two inter-subunit S–S bonds (T_m values of 78.4 °C and 78.3 °C, respectively).

Thermostability was also evaluated by heat inactivation experiments by assaying residual activities of variants after heat treatment for 20 min. As shown in Table 3, the purified wild-type NAAAR retained 50% of initial activity at 65.6 °C, which is referred to as the thermostable temperature. Consistent with the results of higher T_m values, all NAAAR variants also showed elevated thermostable temperatures, particularly V265C, which had a 7 °C increase compared with the wild-type enzyme.

The half-lives of three NAAAR variants at 70 °C were also determined. Whereas wild-type NAAAR lost 50% of its activity in 7 min (Table 3), a significant increase in half-lives was found for A68C-D72C, E149C-A182C and V265C. Notably, V265C had the greatest increase (6.6-fold; 47 min) as compared to ~3.3-fold increases for the other mutants (Table 3). Based on the structure, the inter-subunit bridges of A68C-D72C connect exterior helices of capping domains (H_{C1} of A subunit *versus* H_{C1} of C subunit), while the intra-subunit link in E149C-A182C is located between two exterior helices (H_{B1} of A subunit and H_{B2} of A subunit) of the barrel domain. On the other hand, the intra-subunit S–S link of V265C connects S_{B5} and S_{B6} strands that are situated in the core of the barrel domain. These results together suggest that introduction of either inter or intra-subunit S–S bridges into NAAAR leads to increased structural rigidity, thereby improving thermal resistance. Moreover, the central β-sheet in the barrel domain is the most crucial region in the structural stability.

Table 3. Thermostability of NAAAR and D-NCAase

Variants	Stability		
	T_m (°C)[a]	Thermostable temperature (°C)[b]	Half-lives (h)[c]
NAAAR			
Wild-type	71.9	65.6	0.12
A68C-D72C	78.4	70.8	0.39
P60C-Y100C	78.3	ND[d]	ND
E149C-A182C	75.2	70.4	0.41
V265C	78.8	72.6	0.79
A68C-D72C/ E149C-A182C	79.3	ND	0.81
A68C-D72C/ V265C	80.0	ND	0.88
E149C-A182C/ V265C	78.6	ND	1.44
A68C-D72C/ E149C-A182C/ V265C	78.6	ND	1.34
D-NCAase			
Wild-Type	68.6	63.1	8.1
A302C	77.4	71.0	20.4
P295C-F304C	72.3	64.8	16.2
P178C	68.3	63.6	8.0
A222C	67.8	63.5	9.0

[a] T_m is the transition midpoint of the unfolding curve determined by monitoring ellipticity at 222 nm using circular dichroism.
[b] Temperature at which enzyme retained 50% activity after incubation for 20 min.
[c] Half-lives of thermal inactivation were determined by assaying residual activity as described in Materials and Methods after incubation of NAAAR at 70 °C or D-NCAase at 50 °C.
[d] ND, not determined.

In order to see whether mutations to NAAAR could have an additive effect on thermostability, four mutants containing combinations of the previous substitutions were generated by site-directed mutagenesis: A68C-D72C/E149C-A182C, A68C-D72C/V265C, E149C-A182C/V265C, and A68C-D72C/E149C-A182C/V265C. The purified A68C-D72C/E149C-A182C and A68C-D72C/V265C proteins that combined inter and intra-subunit disulfide bonds were found to have a slightly higher T_m values (Table 3). Much longer half-lives (6.8 and 7.3-fold, respectively) were observed at 70 °C compared with the wild-type NAAAR, indicating that the combinations of those substitutions had a cooperative effect. The E149C-A182C/V265C mutant with two intra-subunit bridges showed the highest half-life at 70 °C (12-fold increase compared to wild-type NAAAR), despite having a similar T_m value to that of V265C. The triple A68C-D72C/E149C-A182C/V265C mutant, however, did not show any further enhanced stability. The relative activities of the four purified mutants were lower than that of the wild-type enzyme (89.3%, 40.9%, 40.2%, and 44.5%, respectively). Subsequent kinetic experiments were thus focused on non-combined variants.

Among the mutant D-NCAases, A302C and P295C-F304C had increased T_m values (increases of 8.8 °C and 3.7 °C, respectively) and thermostable temperatures (increases of 7.9 °C and 1.7 °C, respectively), compared with the wild-type enzyme (Table 3). A302C and P295C-F304C also showed a significant increase in half-lives at 50 °C (2.5-fold and twofold, respectively). These results together suggest that the hydrophobic region formed by the interlocked C-terminal segments near the dyad axis is essential in subunit association and that introduction of S–S bridges at this location is a robust approach to enhance thermostability. On the other hand, mutants P178C and A222C, which did not form the predicted S–S bonds, hardly showed any change. Thus, in line with the results from NAAARs, the engineered D-NCAase mutants with additional S–S bridges are highly resistant to thermal challenge, particularly A302C.

Differences in catalytic activities: NAAARs *versus* D-NCAases

Using *N*-acetyl-L-methionine as substrate, effects of temperature on the enzyme activities of wild-

type and mutant NAAARs were examined. All NAAARs had similar profiles with the highest activities at 55–60 °C except that V265C had relatively lower activities (Figure 5(a)). The kinetic parameters of purified NAAARs were then determined at 50 °C. As shown in Table 4, A68C-D72C that had inter-subunit links had a slightly reduced k_{cat}/K_m ratio as compared to the wild-type NAAAR (0.56 *versus* 0.65). The two mutants that had intra-subunit links, E149C-A182C and V265C, had a decrease in the k_{cat}/K_m ratio, respectively (~28% and ~43% decrease), particularly V265C that had the greatest thermostability.

Examination of the temperature effects on D-NCAases revealed that the wild-type enzyme displayed an optimum activity at ~55 °C, followed by a dramatic decrease above 60 °C (Figure 5(b)). The thermostable mutants P295C-F304C and A302C, interestingly, had much higher specific activities from 55 °C to 70 °C, as compared with the wild-type D-NCAase (Figure 5(b)). Notably, A302C had the highest specific activity at ~65 °C.

We thus further characterized kinetic parameters of the D-NCAases at 37 °C, 55 °C, and 65 °C. All three D-NCAases exhibited similar kinetic parameters at 37 °C (Table 4). A302C, which displayed the highest thermostability, had a slight increase (~16%) in the k_{cat}/K_m ratio compared with the wild-type enzyme. When the temperature was held at 55 °C, each of the three enzymes showed a significantly enhanced k_{cat}/K_m value as compared to 37 °C. It is noted that A302C had a ~47% increase in the k_{cat}/K_m ratio compared with the wild-type enzyme. At 65 °C, the wild-type enzyme dramatically lost its catalytic power (~21% decrease in k_{cat}/K_m value as compared to 37 °C). This is not surprising given that the wild-type enzyme lost 50% of its activity after treatment at 63.1 °C for 20 min. P295C-F304C with the thermostable temperature of 64.8 °C also showed a slightly reduced k_{cat}/K_m value at 65 °C as compared to 55 °C. In contrast, A302C that had the thermostable temperature of 71.0 °C displayed the best k_{cat}/K_m ratio (3.3-fold increase at 65 °C compared with the wild-type enzyme at 37 °C). These results together suggest that A302C is most successful at achieving both enhanced thermostability and thermoactivity.

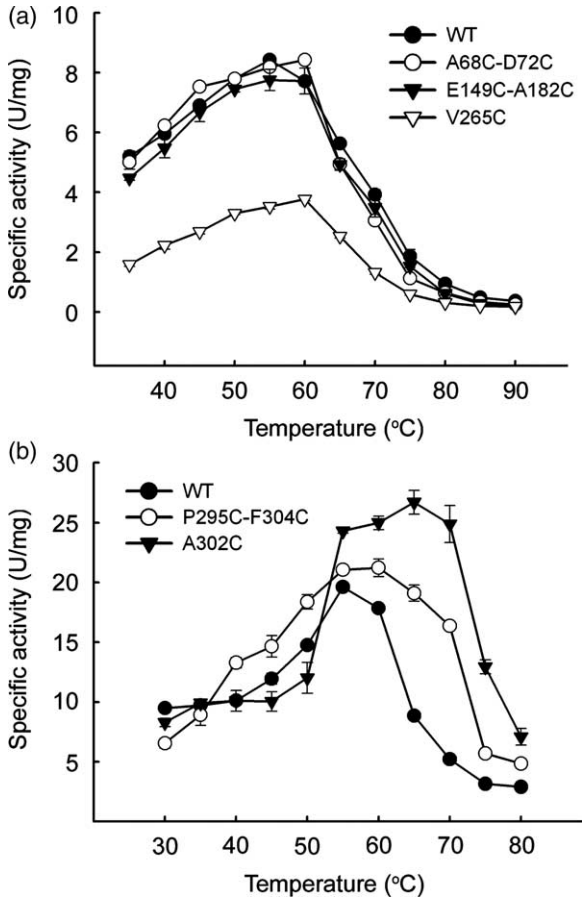

Figure 5. Effects of temperature on the activity of NAAARs (a) and D-NCAases (b). As compared with the wild-type enzyme, mutant NAAARs showed similar profiles except that V265C had relatively lower activities. In contrast, D-NCAase variants, P295C-F304C and A302C had higher activities from 55 70 °C to 70 °C.

Structure–activity relationship of NAAARs

We have investigated the structures and activities of two different enzymes and how they are affected by engineering for enhanced thermostability. Our results demonstrate that the new inter-subunit disulfide cross-links of the NAAAR multimers do not affect the overall structure and result in enhanced thermostability as compared to the wild-type protein. We find that the cross-linked A68C-D72C *apo* structure demonstrates a "liganded-like" conformation and an ordered lid loop over the binding pocket. This is likely a result of reduced thermal fluctuation as introduction of additional S–S bridges into proteins is generally considered to result in more "rigid" structure.

We found that A68C-D72C had comparable catalytic power as the wild-type enzyme, as shown in their similar k_{cat}/K_m ratios and activity–temperature profiles (Figure 5(a)). Similarly for E149C-A182C, the designed mutant that had an additional intra-subunit S–S link showed increased thermostability without compromising catalytic efficiency. These results suggest that similar catalytic efficiency might be expected as long as the introduced site is far from the catalytic residues in NAAAR. On the other hand, the designed V265C mutant showed much lower reactivity, despite the greatest thermostability. Analysis of the wild-type structure reveals that D245 and K269, two critical residues involved in catalysis, are located at the C-terminal ends of the two strands (S_{B5} and S_{B6}, respectively) that would be covalently bridged by the new disulfide bond. Given that NAAAR shows a large induced-fit movement upon substrate binding, one explanation is the reduced conformational flexibility of the cross-linked strands that is required for substrate access and/or product release.[23] This would restrict the motions of these

Table 4. Kinetic parameters of NAAAR and D-NCAase

Variants	Temperature (°C)	Kinetic parameters[a] k_{cat} (min^{-1})	K_m (mM)	k_{cat}/K_m (min^{-1} mM^{-1})
NAAAR				
Wild-type	50	6.85±0.32	10.6±1.1	0.65
A68C-D72C		6.00±0.52	10.8±1.1	0.56
E149C-A182C		5.48±0.45	11.6±1.4	0.47
V265C		4.61±0.58	12.5±2.6	0.37
D-NCAase				
Wild-type	37	473±23	1.32±0.07	359
A302C		464±36	1.12±0.07	414
P295C-F304C		478±22	1.22±0.06	392
Wild-type	55	893±37	1.24±0.08	720
A302C		1145±44	1.08±0.07	1061
P295C-F304C		915±35	1.14±0.07	803
Wild-type	65	416±19	1.47±0.09	283
A302C		1348±39	1.14±0.02	1182
P295C-F304C		823±18	1.16±0.07	710

[a] Kinetic parameters were calculated based on the results of three independent experiments at each temperature.

residues, thereby significantly lowering the enzyme's catalytic power as shown in Table 4.

Structure–activity relationship of D-NCAases

D-NCAase shows limited structural changes with or without a ligand, indicating a less flexible protein. The substitution at residue 302, which is at a distance of around 24 Å from the catalytic residue (A302(C^{β})–C172(S^{γ})), does not perturb either the overall structure or the active-site arrangement. A striking finding in this work is that the single A302C mutant not only displays enhanced thermostability but also elevated catalytic properties at higher temperatures (Table 4 and Figure 5(b)). Another mutant P295C-F304C, which contains two point mutations near residue 302, also showed improved thermostability and enhanced activity at higher temperatures. The increased thermostability of A302C can be accounted for by the reduced positional fluctuations or the increased conformational rigidity due to the presence of the disulfide bridges between the subunits. Indeed, the growing experimental data have suggested that conformational rigidity is a prerequisite for high protein thermostability.[9]

The enhanced enzymatic activity of A302C as compared with that of the native enzyme at higher temperatures is interesting. We have thus investigated the dynamic behaviors for the dimeric form of D-NCAases, since this enzyme exists as a dimer in solution.[28] Figure 6 shows the r.m.s. fluctuations (RMSFs) for both the wild type and A302C at 300 K, 338 K, and 350 K. We observe that the RMSFs of the catalytic residues, i.e. E47, K127, and C172, are generally much smaller than those of other non-catalytic residues. In parallel with the catalytic residues, we also observe that their neighboring residues (within 4 Å) show relatively smaller fluctuations. This is consistent with the recent study by Yang & Bahar[32] that the catalytic residues have significantly lower positional fluctuations than

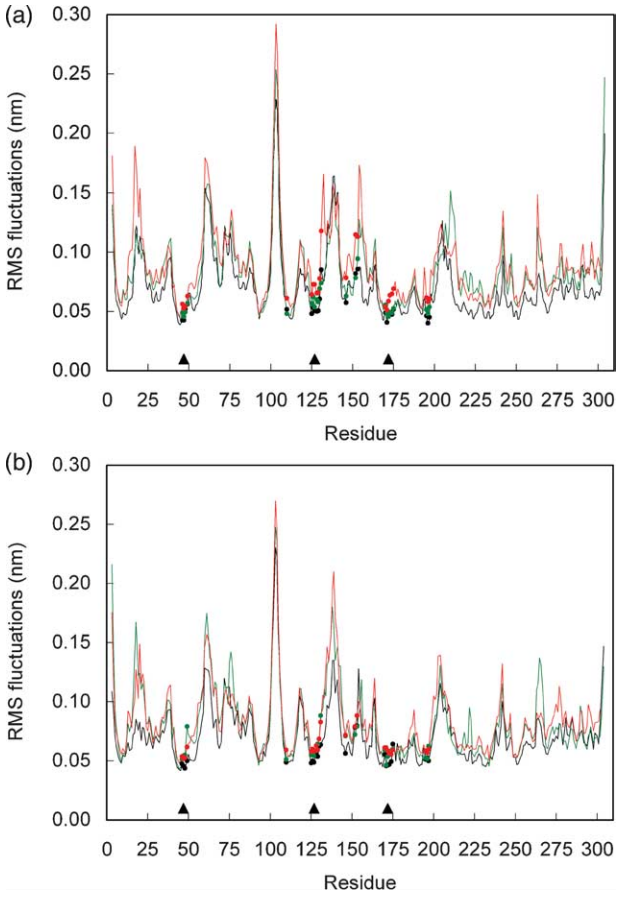

Figure 6. (a) Root-mean-square fluctuations of C^{α} atoms calculated for the D-NCAase dimer from the 2 ns molecular dynamic simulation at 300 K (black line), 338 K (green line) and 350 K (red line). (b) r.m.s. fluctuations of C^{α} atoms calculated for the A302C D-NCAase dimer from the 2 ns molecular dynamic simulation at 300 K (black line), 338 K (green line) and 350 K (red line). The positions of the catalytic residues, i.e. E47, K127, and C172, are marked by filled triangles. The residues that are within 4 Å of the catalytic resiudes are marked by filled circles.

other non-catalytic residues. Apparently, enzymatic activity is associated with the low translational mobility of the catalytic residues, which helps maintain the fine-tuned catalytic architecture. As expected, the RMSFs of all residues become larger for both enzymes at higher temperatures. Of interest, when temperature increases, the relative changes in RMSFs for the catalytic region of the wild-type (Figure 6(a)) are much larger than those of A302C (Figure 6(b)). These results suggest that A302C with the inter-subunit covalent bridge can well sustain the fine-tuned design of active sites even at higher temperature like 350 K, thereby improving catalytic activity.

Because of its pharmaceutical importance, engineering of D-NCAase for high thermostability has previously been attempted with varying degrees of success. In a previous study, an *Agrobacterium* sp. strain KNK712 D-NCAase mutant that had combinations of three substitution sites (H57Y, P203E, and V236A) derived from a mutagenesis study showed a significantly improved thermostability (it had 50% of the initial activity after incubation for 10 min at 75 °C).[33,34] However, the binding affinity and the V_{max} value were reduced (~40% and 16%, respectively), yielding a less efficient enzyme. Using the directed evolution approach, another study found that the best thermostable mutant consisted of six substitution sites in *A. tumefaciens* NRRL B11291 D-NCAase.[35] Although this mutant had 50% of the initial activity after incubation for 30 min at 73 °C, compared with 61 °C for the wild-type enzyme, the k_{cat}/K_m value was also reduced (~28% decrease) due to the lower k_{cat}. These mutants were noted to contain one or several mutation sites located inside the core of the protein or near the active-site region that might affect subtle changes of the active-site arrangement and dynamics, as opposed to the remote location of residue 302 from the active center in the present study.

In conclusion, our results demonstrate that introduction of inter-subunit S–S bridges is a feasible and robust approach to increase the desired thermostability without losing catalytic efficiency as long as the active-site remains viable. Furthermore, the engineered D-NCAase mutants with cross-linked C-terminal regions enhance enzymatic activity at higher temperatures, possibly by sustaining the fine-tuned design of active sites. These mutants possess both enhanced thermostability and enhanced thermoactivity.

Materials and Methods

Site-directed mutagenesis

Site-directed mutagenesis was performed essentially using the overlap extension PCR method.[36] For each mutation, two PCR fragments having overlapping ends were generated using two sets of two 24 base-pair primers, respectively: (i) a primer located in the vector, upstream from the T7 promoter and the 6 His tag and a primer that contained the mutation; and (ii) a primer located downstream from the C terminus of the gene and a primer that contained the same mutation on the complementary strand. The resulting two fragments were gel-purified (Geneaid) and then used in the second step that included a third PCR using the two primers located in the vector. The resulting PCR product was digested with BamHI-HindIII and cloned directly into pQE30. All the mutations were confirmed by sequencing of the whole ligated PCR fragment.

Expression and purification of wild-type and mutant enzymes

Recombinant enzymes expressed in *E. coli* JM109 cells were isolated as described.[23,37] Bacterial pellets were fractionated and soluble proteins in cytosolic fractions were collected. The expressed protein with a His_6 tag was purified by immobilized cobalt ion chromatography and then analyzed by SDS-PAGE to verify the purity. The protein concentration was assayed according to the Bradford method with bovine serum albumin as a standard.[38]

Enzyme activity assay

Wild-type and mutant NAAAR activities were determined essentially according to Tokuyama *et al.*[39,40] In brief, an appropriate amount of enzyme was incubated with 0.05 M Tris–HCl buffer (pH 8.0), 1 mM cobalt chloride, and 10 mM *N*-acetyl-L-methionine at 50 °C for 30 min, followed by boiling for 5 min to stop the reaction. The final mixtures were separated and measured by HPLC on a ChiroBiotic T column (Astec). Kinetic parameters, K_m (mM) and k_{cat} (min^{-1}) values were determined from initial velocity data with varying concentrations of *N*-acetyl-L-methionine (2–20 mM). To determine the effects of temperature on NAAAR activity, each purified enzyme was incubated in the reaction solution for 20 min at various temperatures (from 35 °C to 90 °C). At the end of the incubation, the reaction mixtures were heated on boiling water to stop the reaction, followed by the HPLC analysis as described above.

For D-NCAase, the activity was assayed by monitoring the release of ammonium product, which can be converted to colored indophenol complexes by the Bertholet reaction and spectrophotometrically quantitated at 625 nm.[41] The K_m (mM) and k_{cat} (min^{-1}) values for wild-type and mutant D-NCAase were determined from initial velocity data in reactions containing enzyme, 100 mM sodium phosphate buffer (pH 7.0, 37 °C), 5 mM EDTA with varying concentrations of *N*-carbamoyl-D-*p*-hydroxyphenylglycine (0.5–10 mM). To determine the effects of temperature on D-NCAase activity, each purified enzyme was incubated in the reaction solution for 20 min at various temperatures (from 30 °C to 80 °C). At the end of the incubation, reaction mixtures were heated on boiling water to stop the reaction, and ammonium product was detected by the standard method described above.

Thermal denaturation by circular dichroism analysis

Circular dichroism (CD) experiments were performed on an AVIV CD spectropolarimeter (model 62A DS). Scans were performed from 200 nm to 260 nm (0.1 cm path length) with NAAAR protein at a concentration of

0.5 mg ml^{-1} in 50 mM Tris–HCl (pH 8.0), or D-NCAase protein at a concentration of 0.5 mg ml^{-1} in 10 mM Hepes (pH 7.0). All data were determined as the average of three scans. The change in ellipticity at 222 nm was monitored as the protein sample was heated from 20 °C to 96 °C in 2 deg. C increments at a heating rate of 5 °C min^{-1}. Each unfolding curve was smoothed and normalized using the program AVIV software V2.90. Apparent T_m values were determined from the transition midpoints of the unfolding curves.

Thermal inactivation

Sample solutions containing purified NAAAR protein (0.04 mg ml^{-1}) in 50 mM Tris–HCl were treated at 70 °C for different time intervals. Aliquots were withdrawn, chilled on ice immediately, and assayed for residual enzyme activity using the standard method as described above. Half-lives of each NAAAR protein at 70 °C were derived at which the enzyme retained 50% of activity.

Heat inactivation experiments were also performed with sample solutions containing purified NAAAR protein (0.04 mg ml^{-1}) in 50 mM Tris–HCl at different temperatures (ranging from 40 °C to 90 °C) for 20 min. The temperature at which an enzyme retained 50% of activity after heat treatment for 20 min was referred as the thermostable temperature.

For D-NCAase, similar procedures were performed with sample solutions containing purified D-NCAase protein (0.06 mg ml^{-1}) in 100 mM sodium phosphate. Half-lives of D-NCAases were determined at 50 °C. The thermostable temperature was derived when sample solutions were treated at different temperatures (ranging from 37 °C to 80 °C) for 20 min.

Crystallization and data collection

Crystallization of NAAAR mutants was conducted using the vapor diffusion method in hanging drops of protein solution (10 mg ml^{-1} in 50 mM Tris–HCl (pH 8.0)) at constant room temperature.[23] Four mutants (A68C-D72C, E149C-A182C, Y218C, and G127C-T313C) were crystallized in 0.24 M lithium sulfate, 28%–36% (w/v) PEG 4000, and 100 mM Tris–HCl buffer (pH 8.5). A68C-D72C liganded complex crystals could not be obtained by soaking with NAQ. Complex crystals were instead obtained by co-crystallization with 2.5 mM NAQ and 2.5 mM $MgCl_2$ under a condition that contains 0.24 M lithium sulfate, 28%–36% (w/v) PEG 4000, 0.1 M Tris–HCl (pH 8.5) for three to six days. The crystals grow as a diamond and reach their maximum size within a week at room temperature. All mutant crystals belong to space group *P*4 with comparable unit cell dimensions to those of the wild-type NAAAR and contain four molecules per asymmetric unit (see Table 2).

D-NCAase crystals were obtained by the hanging-drop vapor diffusion method using protein solutions containing ~15 mg/ml protein with precipitating solution at room temperature as described.[37] A222C and A302C mutants were initially grown as micro-crystals with the precipitating condition of 1.20 M lithium sulfate and 0.1 M Hepes buffer (pH 7.0). A micro-seeding method was then applied to obtain large single crystals. For P295C-F304C and P178C, no crystals were obtained. All crystals belong to space group $P2_1$ with unit cell dimensions comparable to those of wild-type D-NCAase (Table 2). There are four molecules per asymmetric unit.

Prior to data collection, crystals were transferred to mineral oil for a few seconds and then flash-frozen in a liquid nitrogen stream. Data from crystals of NAAAR mutants (E149C-A182C, G127C-T313C, and Y218C) and D-NCAase mutants (A222C and A302C) were collected at −150 °C using a MSC X-Stream Cryo-system with double-mirror-focused Cu Kα X-ray radiation generated from a Rigaku RU-300 rotating anode generator at the Macromolecular X-ray Crystallographic Laboratory of National Tsing Hua University, Hsinchu, Taiwan. The NAAAR A68C-D72C crystal data were collected on BL12B2 Taiwan beamline at SPring-8, Japan using an ADSC Quantum 4R CCD detector. All data were processed with the HKL/HKL2000 suite.[42] The statistics of the data collections are given in Table 2.

Structure determination and refinement

Wild-type crystal structures, omitting solvent molecules (PDB codes: NAAAR, 1R0M; D-NCAase, 1FO6), were used to calculate a difference Fourier map and calculated phases for each mutant. Clearly visible density for the substituted side-chain in each mutant was observed. A model was thus readily built for each mutant using O version 9.0.7.[43] Crystallographic refinement was carried out using the maximum-likelihood target function embedded in REFMAC 5 and coupled to ARP/wARP.[44,45] Five percent of the reflections were randomly selected and used to compute a free R value (R_{free}) for cross-validation of the model. Sigma A-weighted $2F_o-F_c$ and F_o-F_c maps were generated and inspected after each cycle of refinement to modify the model manually on an interactive computer with the program O. The progress of the refinement was evaluated by the improvement in the quality of the maps, as well as the reduced values for R and R_{free}. Geometrical restraints were then applied and gradually relaxed during the refinement. The stereochemistry of each protein model was assessed using the program PROCHECK.[46] A summary of refinement statistics is shown in Table 2.

Atomic coordinates

The coordinates and structure factors of NAAARs (A68C-D72C, A68C-D72C·NAQ, E149C-A182C, G127C-T313C, Y218C) and D-NCAases (A302C and A222C) have been deposited in the RCSB Protein Data Bank with accession codes 2GGG, 2GGH, 2GGI, 2FKP, 2GGJ, 2GGK, and 2GGL, respectively.

Structural comparisons

Comparisons between wild-type and mutant structures were carried out with the program LSQMAN in O[47] by superimposing the C^α atoms of monomers or subdomains. Images of three-dimensional structure models were prepared with MOLSCRIPT[48] coupled to Raster3D.[49] Structure Figures with electron density maps were prepared with PyMOL†.

Molecular dynamic simulations

The starting structures for the simulations were from PDB 1FO6 and 2GGK. All simulations were performed with the GROMACS 3.3 program,[50,51] running on Fedora

† www.pymol.org

Linux system. The GROMOS 96 43a1 force field was used. The structures were solvated in a box of a size 9.501 nm × 9.387 nm × 6.324 nm containing 15,136 SPC water molecules. The long range electrostatic interactions were computed by the smooth particle-mesh Ewald (PME) algorithm.[52,53] The full direct and reciprocal space parts were calculated with a Fourier spacing of 0.12 nm and the direct space part of the electrostatic interaction was cut off at 0.9 nm. The Lennard-Jones interaction was calculated using a cut-off of 1.4 nm. Newton's equations of motion were integrated with a time step of a 2 fs. All bond lengths were constrained using LINCS.[54] The system was coupled to a temperature bath using Berendsen's algorithm.[55] All simulations with the wild-type or A302C D-NCAases were carried out for 2 ns at 300 K, 338 K, and 350 K, respectively. The first 1 ns run was used to attain equilibrium, while the trajectories of the last 1 ns were used for analysis.

Acknowledgements

We thank the Macromolecular X-ray Crystallographic Center of NTHU Instrument Center at Hsinchu, National Tsing Hua University, Taiwan, and the BL12B2 Taiwan beamline at SPring-8, Japan for access to their facilities for data collection. This work was supported by grants from NSC, Taiwan (NSC93-2313-B-007-001 and NSC94-2313-B-007-002).

References

1. Matthews, B. W. (1995). Studies on protein stability with T4 lysozyme. *Advan. Protein Chem.* **46**, 249–278.
2. Arnold, F. H., Wintrode, P. L., Miyazaki, K. & Gershenson, A. (2001). How enzymes adapt: lessons from directed evolution. *Trends Biochem. Sci.* **26**, 100–106.
3. Morley, K. L. & Kazlauskas, R. J. (2005). Improving enzyme properties: when are closer mutations better? *Trends Biotechnol.* **23**, 231–237.
4. Parales, R. E. & Ditty, J. L. (2005). Laboratory evolution of catabolic enzymes and pathways. *Curr. Opin. Biotechnol.* **16**, 315–325.
5. Wei, C. L., Yang, Y. B., Wang, W. C., Liu, W. C., Hsu, J. S. & Tsai, Y. C. (2003). Engineering *Streptomyces clavuligerus* deacetoxycephalosporin C synthase for optimal ring expansion activity toward penicillin G. *Appl. Environ. Microbiol.* **69**, 2306–2312.
6. Eijsink, V. G., Bjork, A., Gaseidnes, S., Sirevag, R., Synstad, B., van den Burg, B. & Vriend, G. (2004). Rational engineering of enzyme stability. *J. Biotechnol.* **113**, 105–120.
7. Jaenicke, R. & Bohm, G. (1998). The stability of proteins in extreme environments. *Curr. Opin. Struct. Biol.* **8**, 738–748.
8. Demirjian, D. C., Moris-Varas, F. & Cassidy, C. S. (2001). Enzymes from extremophiles. *Curr. Opin. Chem. Biol.* **5**, 144–151.
9. Vieille, C. & Zeikus, G. J. (2001). Hyperthermophilic enzymes: sources, uses, and molecular mechanisms for thermostability. *Microbiol. Mol. Biol. Rev.* **65**, 1–43.
10. Van den Burg, B., Vriend, G., Veltman, O. R., Venema, G. & Eijsink, V. G. (1998). Engineering an enzyme to resist boiling. *Proc. Natl Acad. Sci. USA*, **95**, 2056–2060.
11. Trejo, F., Gelpi, J. L., Ferrer, A., Boronat, A., Busquets, M. & Cortes, A. (2001). Contribution of engineered electrostatic interactions to the stability of cytosolic malate dehydrogenase. *Protein Eng.* **14**, 911–917.
12. Walden, H., Bell, G. S., Russell, R. J., Siebers, B., Hensel, R. & Taylor, G. L. (2001). Tiny TIM: a small, tetrameric, hyperthermostable triosephosphate isomerase. *J. Mol. Biol.* **306**, 745–757.
13. Thoma, R., Hennig, M., Sterner, R. & Kirschner, K. (2000). Structure and function of mutationally generated monomers of dimeric phosphoribosylanthranilate isomerase from *Thermotoga maritima*. *Struct. Fold. Des.* **8**, 265–276.
14. Clantin, B., Tricot, C., Lonhienne, T., Stalon, V. & Villeret, V. (2001). Probing the role of oligomerization in the high thermal stability of *Pyrococcus furiosus* ornithine carbamoyltransferase by site-specific mutants. *Eur. J. Biochem.* **268**, 3937–3942.
15. Flores, H. & Ellington, A. D. (2002). Increasing the thermal stability of an oligomeric protein, beta-glucuronidase. *J. Mol. Biol.* **315**, 325–337.
16. Maeda, N., Kanai, T., Atomi, H. & Imanaka, T. (2002). The unique pentagonal structure of an archaeal Rubisco is essential for its high thermostability. *J. Biol. Chem.* **277**, 31656–31662.
17. Gokhale, R. S., Agarwalla, S., Francis, V. S., Santi, D. V. & Balaram, P. (1994). Thermal stabilization of thymidylate synthase by engineering two disulfide bridges across the dimer interface. *J. Mol. Biol.* **235**, 89–94.
18. Velanker, S. S., Gokhale, R. S., Ray, S. S., Gopal, B., Parthasarathy, S., Santi, D. V., Balaram, P. & Murthy, M. R. (1999). Disulfide engineering at the dimer interface of *Lactobacillus casei* thymidylate synthase: crystal structure of the T155C/E188C/C244T mutant. *Protein Sci.* **8**, 930–933.
19. Bogin, O., Levin, I., Hacham, Y., Tel-Or, S., Peretz, M., Frolow, F. & Burstein, Y. (2002). Structural basis for the enhanced thermal stability of alcohol dehydrogenase mutants from the mesophilic bacterium *Clostridium beijerinckii*: contribution of salt bridging. *Protein Sci.* **11**, 2561–2574.
20. Bjork, A., Dalhus, B., Mantzilas, D., Eijsink, V. G. & Sirevag, R. (2003). Stabilization of a tetrameric malate dehydrogenase by introduction of a disulfide bridge at the dimer–dimer interface. *J. Mol. Biol.* **334**, 811–821.
21. Bjork, A., Mantzilas, D., Sirevag, R. & Eijsink, V. G. (2003). Electrostatic interactions across the dimer–dimer interface contribute to the pH-dependent stability of a tetrameric malate dehydrogenase. *FEBS Letters*, **553**, 423–426.
22. Kabashima, T., Li, Y., Kanada, N., Ito, K. & Yoshimoto, T. (2001). Enhancement of the thermal stability of pyroglutamyl peptidase I by introduction of an intersubunit disulfide bond. *Biochim. Biophys. Acta*, **1547**, 214–220.
23. Wang, W. C., Chiu, W. C., Hsu, S. K., Wu, C. L., Chen, C. Y., Liu, J. S. & Hsu, W. H. (2004). Structural basis for catalytic racemization and substrate specificity of an *N*-acylamino acid racemase homologue from *Deinococcus radiodurans*. *J. Mol. Biol.* **342**, 155–169.
24. Tokuyama, S. & Hatano, K. (1996). Overexpression of the gene for *N*-acylamino acid racemase from *Amycolatopsis* sp. TS-1-60 in *Escherichia coli* and continuous production of optically active methionine by a bioreactor. *Appl. Microbiol. Biotechnol.* **44**, 774–777.
25. Babbitt, P. C., Hasson, M. S., Wedekind, J. E., Palmer, D. R., Barrett, W. C., Reed, G. H. *et al.* (1996).

The enolase superfamily: a general strategy for enzyme-catalyzed abstraction of the alpha-protons of carboxylic acids. *Biochemistry*, **35**, 16489–16501.
26. Olivieri, R., Fascetti, E., Angelini, L. & Degen, L. (1981). Microbial transformation of racemic hydantoins to D-amino acids. *Biotechnol. Bioeng.* **23**, 2173–2183.
27. Takahashi, S., Ohashi, T., Kii, Y., Kumagai, H. & Yamada, H. (1979). Microbial transformation of hydantoins to *N*-carbamyl-D-amino acids. *J. Ferment. Technol.* **57**, 328–332.
28. Wang, W. C., Hsu, W. H., Chien, F. T. & Chen, C. Y. (2001). Crystal structure and site-directed mutagenesis studies of *N*-carbamoyl-D-amino-acid amidohydrolase from *Agrobacterium radiobacter* reveals a homotetramer and insight into a catalytic cleft. *J. Mol. Biol.* **306**, 251–261.
29. Nakai, T., Hasegawa, T., Yamashita, E., Yamamoto, M., Kumasaka, T., Ueki, T. *et al*. (2000). Crystal structure of *N*-carbamyl-D-amino acid amidohydrolase with a novel catalytic framework common to amidohydrolases. *Structure*, **8**, 729–739.
30. Chen, C. Y., Chiu, W. C., Liu, J. S., Hsu, W. H. & Wang, W. C. (2003). Structural basis for catalysis and substrate specificity of *Agrobacterium radiobacter N*-carbamoyl-D-amino acid amidohydrolase. *J. Biol. Chem.* **278**, 26194–26201.
31. Daniel, R. M., Dunn, R. V., Finney, J. L. & Smith, J. C. (2003). The role of dynamics in enzyme activity. *Annu. Rev. Biophys. Biomol. Struct.* **32**, 69–92.
32. Yang, L. W. & Bahar, I. (2005). Coupling between catalytic site and collective dynamics: a requirement for mechanochemical activity of enzymes. *Structure*, **13**, 893–904.
33. Ikenaka, Y., Nanba, H., Yajima, K., Yamada, Y., Takano, M. & Takahashi, S. (1998). Relationship between an increase in thermostability and amino acid substitutions in *N*-carbamyl-D-amino acid amidohydrolase. *Biosci. Biotechnol. Biochem.* **62**, 1672–1675.
34. Ikenaka, Y., Nanba, H., Yajima, K., Yamada, Y., Takano, M. & Takahashi, S. (1999). Thermostability reinforcement through a combination of thermostability-related mutations of *N*-carbamyl-D-amino acid amidohydrolase. *Biosci. Biotechnol. Biochem.* **63**, 91–95.
35. Oh, K. H., Nam, S. H. & Kim, H. S. (2002). Improvement of oxidative and thermostability of *N*-carbamyl-D-amino acid amidohydrolase by directed evolution. *Protein Eng.* **15**, 689–695.
36. Ho, S. N., Hunt, H. D., Horton, R. M., Pullen, J. K. & Pease, L. R. (1989). Site-directed mutagenesis by overlap extension using the polymerase chain reaction. *Gene*, **77**, 51–59.
37. Hsu, W. H., Chien, F. T., Hsu, C. L., Wang, T. C., Yuan, H. S. & Wang, W. C. (1999). Expression, crystallization and preliminary X-ray diffraction studies of *N*-carbamyl-D-amino-acid amidohydrolase from *Agrobacterium radiobacter*. *Acta Crystallog. sect. D*, **55**, 694–695.
38. Bradford, M. M. (1976). A rapid and sensitive method for the quantitation of microgram quantities of protein utilizing the principle of protein–dye binding. *Anal. Biochem.* **72**, 248–254.
39. Tokuyama, S. & Hatano, K. (1994). Discovery of a novel enzyme, *N*-acylamino acid racemase in an actinomycete: screening, isolation, and identification. *Biosci. Biotechnol. Biochem.* **58**, 24–27.
40. Tokuyama, S., Miya, H., Hatano, K. & Takahashi, T. (1994). Purification and properties of a novel enzyme, *N*-acylamino acid racemase, from *Strpetomyces atratus* Y-53. *Appl. Microbiol. Biotechnol.* **40**, 835–840.
41. Gordon, S. A., Fleck, A. & Bell, J. (1978). Optimal conditions for the estimation of ammonium by the Berthelot reaction. *Ann. Clin. Biochem.* **15**, 270–275.
42. Otwinowski, Z. & Minor, W. (1997). Processing of X-ray diffraction data collected in oscillation mode. *Methods Enzymol.* **276**, 307–326.
43. Jones, T. A., Zou, J. Y., Cowan, S. W. & Kjeldgaard, M. (1991). Improved methods for building protein models in electron density maps and the location of errors in these models. *Acta Crystallog. sect. A*, **47**, 110–119.
44. Murshudov, G. N., Vagin, A. A. & Dodson, E. J. (1997). Refinement of macromolecular structures by the maximum-likelihood method. *Acta Crystallog. sect. D*, **53**, 240–255.
45. Perrakis, A., Morris, R. & Lamzin, V. S. (1999). Automated protein model building combined with iterative structure refinement. *Nature Struct. Biol.* **6**, 458–463.
46. Laskowski, R. A., MacArthur, M. W., Moss, D. S. & Thornton, J. M. (1993). PROCHECK: a program to check the stereochemical quality of protein structures. *J. Appl. Crystallog.* **26**, 283–291.
47. Kleywegt, G. J. & Jones, T. A. (1997). Defecting folding motifs and similarities in protein structures. *Methods Enzymol.* **277**, 525–545.
48. Kraulis, P. J. (1991). MOLSCRIPT: a program to produce both detailed and schematic plots of protein structures. *J. Appl. Crystallog.* **24**, 946–950.
49. Merrit, E. A. & Murphy, M. E. P. (1994). Raster3D version 2.0. A program for photorealistic molecular graphics. *Acta Crystallog. sect. D*, **50**, 869–873.
50. Berendsen, H. J. C., van der Spoel, D. & van Drunen, R. (1995). GROMACS: a message passing parallel molecular dynamics implementation. *Comp. Phys. Commun.* **91**, 43–56.
51. Lindahl, E. H. B. & van der Spoel, D. (2001). GROMACS 3.0: a package for molecular simulation and trajectory analysis. *J. Mol. Model.* **7**, 306–317.
52. Essmann, U., Perera, L., Berkowitz, M. L., Darden, T., Lee, H. & Pedersen, L. G. (1995). A smooth particle mesh Ewald method. *J. Chem. Phys.* **103**, 8577–8593.
53. Darden, T., York, D. & Pedersen, L. G. (1993). Particle mesh Ewald: an $N \log(N)$ method for Ewald sums in large systems. *J. Chem. Phys.* **98**, 10089–10092.
54. Hess, B. B. H, Berendsen, H. J. C. & Fraaije, J. G. E. M. (1997). LINCS: a linear constraint solver for molecular simulations. *J. Comp. Chem.* **18**, 1463–1472.
55. Berendsen, H. J. C., Postma, J. P., DiNola, A. & Haak, J. R. (1984). MD with coupling to an external bath. *J. Phys. Chem.* **81**, 3684–3690.

Edited by R. Huber

(Received 6 January 2006; received in revised form 27 March 2006; accepted 30 March 2006)
Available online 18 April 2006